

See discussions, stats, and author profiles for this publication at: <https://www.researchgate.net/publication/346621413>

A variational pan-sharpening algorithm to enhance the spectral and spatial details

Article in *International Journal of Image and Data Fusion* · November 2020

DOI: 10.1080/19479832.2020.1838629

CITATION

1

READS

69

3 authors:



Rajesh Gogineni

12 PUBLICATIONS 38 CITATIONS

[SEE PROFILE](#)



Ashvini Chaturvedi

National Institute of Technology Karnataka

24 PUBLICATIONS 124 CITATIONS

[SEE PROFILE](#)



B. S Daya Sagar

Indian Statistical Institute

123 PUBLICATIONS 758 CITATIONS

[SEE PROFILE](#)

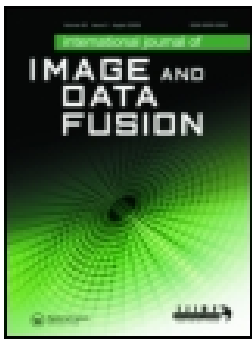
Some of the authors of this publication are also working on these related projects:



SciBase [View project](#)



Journal [View project](#)





A variational pan-sharpening algorithm to enhance the spectral and spatial details

Rajesh Gogineni , Ashvini Chaturvedi & Daya Sagar B S

To cite this article: Rajesh Gogineni , Ashvini Chaturvedi & Daya Sagar B S (2020): A variational pan-sharpening algorithm to enhance the spectral and spatial details, International Journal of Image and Data Fusion, DOI: [10.1080/19479832.2020.1838629](https://doi.org/10.1080/19479832.2020.1838629)

To link to this article: <https://doi.org/10.1080/19479832.2020.1838629>

 [View supplementary material](#) 

 Published online: 02 Nov 2020.

 [Submit your article to this journal](#) 

 [View related articles](#) 

 [View Crossmark data](#) 



ARTICLE



A variational pan-sharpening algorithm to enhance the spectral and spatial details

Rajesh Gogineni^a, Ashvini Chaturvedi^a and Daya Sagar B S^b

^aDepartment of Electronics & Communication Engineering, National Institute of Technology Karnataka, Surathkal, India; ^bSystems Science and Informatics Unit, Indian Statistical Institute-Bangalore Centre, Bangalore, India

ABSTRACT

Pan-sharpening is a remote sensing image fusion technique that generates a high-resolution multispectral (HRMS) image on combining a low resolution multispectral (MS) image and a panchromatic (PAN) image. In this paper, a new optimisation model is proposed for pan-sharpening. The proposed model consists of three terms: (i) a data synthesis fidelity term formulated on inferring the relationship between source MS image and fused image to preserve the spectral information, (ii) a total generalised variation-based prior term to inject the significant spatial details from PAN image to pan-sharpened image, and (iii) a spectral distortion reduction term that exploits the correlation between multispectral image bands. To solve the resultant convex optimisation problem, an efficient and convergence guaranteed operator splitting framework based on the alternating direction method of multipliers (ADMM) algorithm is formulated. Finally, the proposed model is experimentally validated using full-resolution and reduced-resolution data. The pan-sharpened outcomes exhibit the potential of the proposed method in enhancing the spatial and spectral quality.

ARTICLE HISTORY

Received 4 May 2020
Accepted 12 October 2020

KEYWORDS

Pan-sharpening; total generalised variation; inter-band correlation; convex optimisation; variational method; alternating direction method of multipliers

1. Introduction

High-resolution multispectral (HRMS) images are immensely useful for a variety of remote sensing applications like environmental monitoring, change detection (Hussain *et al.* 2013), land-use classification (Chen *et al.* 2017) and land-use extraction (Li *et al.* 2016). The physical and technological constraints restrict the satellite sensors to capture the scenes and subsequently act as a barrier in generating images with high spatial and rich spectral information. Most of the earth observation satellites like, QuickBird, IKONOS, and WorldView provide a high-resolution panchromatic (PAN) image and a low-resolution multispectral (MS) image with several bands. The desired HRMS image can be realised by the fusion of PAN and MS images, and a conventional mechanism that combines the complementary spatial and spectral features is popularly known as Pan-sharpening (PS).

The objective of the pan-sharpening process is to produce a fused image with the spatial characteristics of the PAN image while maintaining spectral consistency with the

CONTACT Rajesh Gogineni ✉ rgogineni9@gmail.com Department of Electronics & Communication Engineering, National Institute of Technology Karnataka, Surathkal 575025, India

Supplemental data for this article can be accessed [here](#).

© 2020 Informa UK Limited, trading as Taylor & Francis Group

low-resolution MS image. Various pan-sharpening methods have been proposed in the last three decades (Xu *et al.* 2014, Vivone *et al.* 2015, Ghassemian 2016, Ma *et al.* 2019), and can be grouped into three categories as component substitution (CS) methods, multi-resolution analysis (MRA) methods, and sparse representation (SR) based techniques.

The basis of CS methods relies upon the transformation of MS image on to space where it is decomposed into its constituent spatial and spectral components and subsequently replacing so obtained spatial component with PAN image. Following which invoking the inverse transformation produces the pan-sharpened image. Intensity-hue-saturation (IHS) (Tu *et al.* 2001, Ling *et al.* 2007), adaptive IHS (AIHS) (Rahmani *et al.* 2010), principal component analysis (PCA)(Chavez *et al.* 1991), Gram–Schmidt (GS) transform (Laben and Brower 2000), GS adaptive (GSA) (Aiazzi *et al.* 2007), band dependent spatial detail (BDSD) are few of the important CS-based methods. The CS methods are known for outcomes having salient features as higher spatial quality (Zhou *et al.* 2014) and less computational complexity. The difference in the spectral response of PAN image and MS image bands leads to colour distortion in CS class of methods.

The MRA methods are based on extracting the spatial details from PAN image using diversified transforms like wavelets, Laplacian pyramid (LP), curvelets, contourlets, and so on. The pan-sharpened image is obtained by injecting the spatial details derived from the PAN image into low-resolution MS bands. The hypothesis of MRA-based methods is widely designated as *Amélioration de la Résolution Spatiale par Injection de Structures* (ARSIS) (Ranchin *et al.* 2003). The well-known MRA methods are wavelet (Amolins *et al.* 2007), additive wavelet luminance proportional (AWLP) (Otazu *et al.* 2005), modulation transfer function based (Aiazzi *et al.* 2006), contourlet (Saeedi and Faez 2011) and so on. The MRA-based methods are recognised for preserving the spectral features compared to the CS-based methods, though MRA methods yield spatial artefacts.

In the recent past, sparse representation (SR) models have been explored as a prominent scheme for pan-sharpening. The first successful attempt made by Li and Yang (Li and Yang 2011) adapted the SR theory for pan-sharpening by constructing a random patches dictionary. The SR-based pan-sharpening methods can be categorised depending upon how the dictionary construction mechanism takes place. The two significant classes are; PS methods in which dictionary is synthesised using the source PAN and MS images (Jiang *et al.* 2012, Li *et al.* 2013, Cheng *et al.* 2014) and other class in which the dictionary is generated utilising the PAN image and its low-resolution version (Zhu and Bamler 2013, Jiang *et al.* 2014, Vicinanza *et al.* 2015). In addition to this, for the mixed PS methods, the principle of MRA combined with SR yields impressive results (Cheng *et al.* 2015, Imani and Ghassemian 2017, Gogineni and Chaturvedi 2018). A single compact dictionary learned from HRMS images is used for pan-sharpening (Ayas *et al.* 2018) to further reduce the complexity in SR-based methods. The utmost concern in the SR model-based methods is designing an appropriate dictionary. Usually, the process of dictionary construction by a conventional training mechanism is computationally expensive. Further, the capability of the dictionary in sparse coding of source image patches is an issue of considerable significance and must be addressed appropriately to develop an efficient pan-sharpening algorithm.

The performance of CS, MRA, and the SR-based pan-sharpening methods is limited in accomplishing a fused outcome while balancing a trade-off between spatial detail enhancement and spectral information retention.

Recently, variational methods (Duran *et al.* 2017) have been evolved as a prominent and attractive alternative for pan-sharpening of multispectral images. The primary concern in the variational model-based pan-sharpening mechanism is to construct objective energy functional with efficient and reliable prior terms. Further, the pan-sharpened outcome is obtained using the energy functional minimisation. The first variational pan-sharpening method, named as pan plus multispectral images (P+XS) was proposed by Ballester *et al.* (Ballester *et al.* 2006). The energy functional is composed of three prior terms, two of these prior terms are defined from the remote sensing image formation model. The third term is based on the geometric information contained in the PAN image. However, P+XS method results in blurring artefacts. The formulation of P+XS has motivated the development of many variational pan-sharpening methods, such as alternate variational pan-sharpening (AVWP) (Möller *et al.* 2012), a nonlocal variational model (NVM) (Duran *et al.* 2014) and a novel variational model for pan-sharpening based on the decomposition of source images into the constituent cartoon and texture components (Lotfi and Ghassemian 2018). In view of discrete formulation, pan-sharpening methods have been proposed based on total variation (TV) as a regulariser (Palsson *et al.* 2014, He *et al.* 2014). Recently, dynamic gradient-based sparsity is exploited for geometric consistency and the method is named as dynamic TV (DTV) (Chen *et al.* 2014). To instigate the feature of sparse representation and to enhance the fidelity of fused image, l_1 -based regularised term is used for pan-sharpening (Chen *et al.* 2018). Most of these variational methods are able to mitigate the spectral distortion. However, these methods induce spatial artefacts like blocks and blurring in the resultant images. In addition to spectral enhancement, a comprehensive model is required to preserve the essential spatial information as well in the fused image.

Over the last few years, deep learning (DL) methods have attracted research community interest and found its applications in various remote sensing paradigms. The representational capability of convolutional neural networks (CNN) in image processing applications, particularly for pan-sharpening of multispectral images has been proven in recent research. An effective PS method based on deep neural networks (DNN) is proposed in (Huang *et al.* 2015). The relationship between LR and HR image patches is mapped by the feed-forward functions. To reconstruct the HRMS image, an impressive back-propagation algorithm is used that trains the entire formulated DNN. Masi *et al.* (Masi *et al.* 2016) proposed a PS method, based on three-layer CNN. This method is simple and competent in preserving the textural features. A fast training CNN (Scarpa *et al.* 2018) is developed to overcome the problem of insufficient data through a target-adaptive tuning phase.

The objective of the pan-sharpening process is to maintain a balanced trade-off between the spatial and spectral information in the fused image. In this paper, a new variational PS method is proposed to inject the most vital spatial features of PAN image into HRMS image, while preserving the essential spectral details. The main contributions of this paper are listed as follows:

(i) A new total generalised variation (TGV) based prior term is proposed to precisely inject the geometric features of PAN image like edges and texture information into the pan-sharpened image. Further, TGV reduces the artefacts and preserves the higher-order smoothness in the fused image.

(ii) By exploiting the correlation between MS image bands, a new spectral distortion minimisation term is designed.

(iii) A data fidelity term is adapted from the image formation model to efficiently inject the spectral details from the source MS image to the pan-sharpened image. According to the image formation model, the LRMS image is considered as a decimated and blurred version of the HRMS image. Under these baseline assumptions, a data generative term is formulated.

(iv) Based on the alternating direction method of multipliers (ADMM), an efficient operator splitting framework is formulated to solve the proposed model.

The rest of the paper is organised as follows: A summary regarding total generalised variation (TGV) and spectral angle mapper (SAM) is presented in [Section 2](#). The proposed variational model for pan-sharpening and subsequently, to solve it an optimisation method is illustrated in [section 3](#). [Section 4](#) presents the experimental results and analysis highlighting the state of key performance measures. [Section 5](#) concludes the paper.

2. Preliminaries

This section presents a necessary mathematical framework of total generalised variation (TGV) and spectral angle mapper (SAM).

2.1. Total generalised variation (TGV)

Total Variation (TV) has been extensively used as a regulariser in image processing applications such as denoising, restoration, and reconstruction. Since TV deals with only first-order derivatives, it leads to undesirable blocky and oil painting artefacts in the resultant image. Total Generalised Variation (TGV) is a generalised version of TV, having the higher-order derivatives. (of order greater than or equal to two). TGV better preserves higher-order smoothness, edges, and eliminates the artefacts in the reconstructed image (Bredies *et al.* 2010).

Let $\Omega \subset \mathbb{R}^d$ be a bounded domain, $C_c^k(\Omega, \text{Sym}^k(\mathbb{R}^d))$ be the space of compactly supported symmetric tensor fields and $\alpha = (\alpha_0, \alpha_1, \dots, \alpha_{k-1}) > 0$ are fixed positive real valued parameters. Then, TGV of order k is defined as:

$$\text{TGV}_\alpha^k(u) = \sup \left\{ \int_\Omega u \text{div}^k v dx \mid v \in C_c^k(\Omega, \text{Sym}^k(\mathbb{R}^d)), \|\text{div}^l v\|_\infty \leq \alpha_l, \quad l = 0, \dots, k-1 \right\}, \quad (1)$$

where $\text{Sym}^k(\mathbb{R}^d)$ is assumed as the space of symmetric tensors on \mathbb{R}^d and v are defined as bounded vector fields. TGV_α^k is referred as total generalised bounded variation of order k with a weight vector $\alpha \in \mathbb{R}^k$. For $k = 1$, $\alpha_0 = 1$ and thus the seminorm TGV_α^k coincides with the bounded variation seminorm.

The space bounded generalised variation (BGV) can be defined as

$$\begin{aligned} \text{BGV}_\alpha^k(\Omega) &= \left\{ u \in L^1(\Omega) \mid \text{TGV}_\alpha^k(u) < \infty \right\}, \\ \|u\|_{\text{BGV}_\alpha^k} &= \|u\|_1 + \text{TGV}_\alpha^k(u). \end{aligned} \quad (2)$$

BGV spans the set of functions of order k with a weight vector α which are the generalised version of bounded variations. TGV_α^k is a seminorm on the normed space BGV_α^k , where the space $\text{BGV}_\alpha^k(W)$ is independent of α .

When $k = 2$, $\text{Sym}^2(\mathbb{R}^d)$ is the space $S^{d \times d}$ that spans all symmetric $d \times d$ matrices and models a set of bilinear forms which are usually symmetric. Specifically, the second-order TGV (with $k = 2$) can be expressed as:

$$\text{TGV}_\alpha^2(u) = \sup \left\{ \int_{\Omega} u \text{div}^2 w dx \mid w \in C_c^2(\Omega, S^{d \times d}), \|w\|_{\infty} \leq \alpha_0, \|\text{div} w\|_{\infty} \leq \alpha_1 \right\}, \quad (3)$$

where the divergences can be defined as:

$$(\text{div} w)_h = \sum_{j=1}^d \frac{\partial w_{hj}}{\partial x_j}, \quad 1 \leq h \leq d, \quad \text{div}^2 w = \sum_{h,j=1}^d \frac{\partial^2 w_{hj}}{\partial x_h \partial x_j}. \quad (4)$$

TGV is a convex function and the polynomials of the order less than $k-1$, the value of the semi-norm, TGV_α^k is zero.

2.2. Spectral angle mapper (SAM)

Given two spectral vectors, in which $\mathbf{v} = \{v_1, v_2, \dots, v_N\}$ be the pixel vector of multi-spectral bands associated with an original image and $\Phi = \{\hat{v}_1, \hat{v}_2, \dots, \hat{v}_N\}$ be the pixel vector of the corresponding fused bands, respectively. Let N be the number of bands present in the image. The spectral angle mapper, SAM is determined as the spectral angle between the two vectors (Alparone *et al.* 2015) as

$$\text{SAM}(\mathbf{v}, \Phi) = \arccos \left(\frac{\langle \mathbf{v}, \Phi \rangle}{\|\mathbf{v}\|_2 \|\Phi\|_2} \right) \quad (5)$$

SAM is generally averaged over the entire image. If the two images used for comparison are spectrally equal then the SAM value is zero, this optimal value is true in an idealistic scenario and it indicates the absence of spectral distortion; however, there exists a possibility of radiometric distortion.

3. Proposed variational model

The proposed variational pan-sharpening model consists of three terms to cater the following objectives: (i) To preserve the spectral information, (ii) to enhance the spatial details and (iii) to reduce the spectral distortion. The terms are designed to attain a pan-sharpened image having desired spatial and spectral features with reference to the given PAN and MS images. The First term is adapted from the conventional remote sensing image formation model, which can be treated as a data synthesising fidelity term. The fidelity term enforces spectral information preservation. To retain the requisite geometric structures and to impart the spatial information from PAN image to HRMS image, TGV-based spatial details preserving term is designed. To reduce the spectral distortion in the fused image, the correlation information among MS bands is exploited. The spectral distortion index, namely, SAM is utilised to design an inter-band correlation term.

There exists a significant difference between the first and third terms in the proposed model. The first term enables the spectral detail transfer in a holistic manner from MS image into the fused image and does not concern with the correlation among the MS bands, whereas the third term is designed based on the definition of quality metric,

namely, spectral angle mapper (SAM). The SAM-based term exploits the correlation between the MS image bands so as to reduce the spectral distortion.

3.1. Data synthesising fidelity term

The remote sensing image formation model is presented abstractly that prepares an underlying theme for the data synthesising fidelity term:

The source image consists of a PAN image ($P \in \mathbb{R}^{M \times N}$) and Y_j , ($j = 1, 2, \dots, B$) be the LRMS image with B bands with each band of size $m \times n$ pixels, where $m = M/4$ and $n = N/4$. The spatial resolution of PAN image is four times that of the MS image. The pan-sharpened image obtained post fusion process is 'B' band HRMS image ($X = (X_1, X_2, \dots, X_B)$) maintaining the spatial resolution of the PAN image having the size of $M \times N$ pixels for each band. Let $\tilde{Y} = (\tilde{Y}_1, \tilde{Y}_2, \dots, \tilde{Y}_B)$ be the up-sampled LRMS image and has the same size as PAN image, P .

The source images P , Y , and the pan-sharpened image X are vectorized for computational purposes. Following the well-established remote sensing image formation model, the low-resolution MS image bands can be treated as decimated and blurred variants of the corresponding HRMS image bands.

$$Y_i = GX_i + v_i, i = 1, 2, \dots, B. \quad (6)$$

where $G = \gamma_i H$ is the matrix representing blurring, the sensor integration function, and the spatial subsampling. Let γ_i is the blur filter for i^{th} band, and H is the decimation matrix. The blur filter for each band is realised based on the modulation transfer function (MTF) of the band with its respective cut-off frequency. The decimation matrix, $H = \frac{1}{16} \cdot I_4 \otimes ((I_n \otimes 1_{4 \times 1}^T) \otimes (I_m \otimes 1_{4 \times 1}^T))$ is of $(4mn \times 4MN)$ size to perform the downsampling operation and v_i is an additive Gaussian noise matrix for i^{th} band. The operator \otimes denotes Kronecker product. I_4 is an identity matrix of size 4×4 and $1_{4 \times 1}$ is a 4×1 vector with all entries as unity.

Hence, to preserve the spectral details of the LRMS image, the data synthesising fidelity term can be formulated as:

$$J_1(X) = \frac{1}{2} \sum_{i=1}^B \|Y_i - GX_i\|_2^2 \quad (7)$$

where 'l' denotes the number of constituent spectral bands of LRMS/HRMS images.

3.2. Spatial details preserving term

To inject the vital geometric features like edges and rich texture information of the PAN image into the pan-sharpened image, TGV is adapted as regulariser in the proposed algorithm.

The TGV has been used in the reconstruction of images acquired from different modalities like medical images, fusion of visible and infrared images, etc. In addition to the features that are recovered by the TV, the regularisation using TGV predominantly refrains the typical artefacts like oil painting effects.

TGV² (Bredies and Valkonen 2011) can be reformulated as:

$$TGV_{\alpha}^2(u) = \min_{u \in BGV_{\alpha}^k(\Omega), r \in BD(\Omega)} \alpha_1 \int_{\Omega} |u - r| + \alpha_0 \int_{\Omega} |\varepsilon(r)|, \quad (8)$$

With $BGV = \{u \in \Omega / TGV_{\alpha}^k(u) < \infty\}$ is called the space of bounded generalised variation of order k , with weight vector α , where r are the vector fields of bounded deformation, i.e. their distributional symmetrised derivative $\varepsilon(r)$ is a measure and u represents the gradient of vector u .

In order to solve the energy function efficiently using the minimiser called Alternating direction method of multiplier (ADMM), the discretized version of TGV^2 is developed in (Bredies *et al.* 2010).

$$TGV^2(u) = \min_r \alpha_1 \|u - r\|_1 + \alpha_0 \|\varepsilon(r)\|_1 \quad (9)$$

Here, $u = \begin{bmatrix} \partial_x u \\ \partial_y u \end{bmatrix}$ and $\varepsilon(r) = \frac{1}{2} [r + r^T]$ denotes symmetrised derivative. In the proposed method, r represents the processed image. In order to efficiently solve the Eq.9, the directional derivative u is approximated with Du . Where $D = (D_1; D_2)$. Hence,

$$\varepsilon(r) = \begin{bmatrix} D_1 r_1 & \frac{1}{2}(D_2 r_1 + D_1 r_2) \\ \frac{1}{2}(D_2 r_1 + D_1 r_2) & D_2 r_2 \end{bmatrix} \quad (10)$$

where the finite forward differences in x and y directions are measured by the circulant matrices D_1 and D_2 , respectively. Based on the reformulation of TGV , the spatial difference between HRMS image and PAN image is expressed as:

$$J_2(X) = \alpha_1 \sum_{i=1}^N \|D(X_i - P) - r\|_1 + \alpha_0 \|\varepsilon(r)\|_1 \quad (11)$$

The performance eminence of TGV over the conventional TV in preserving textures, edges, and reducing staircase effects has been presented experimentally for different imaging modalities in (Knoll *et al.* 2011, Guo *et al.* 2014a).

3.3. Inter-band correlation preserving term

The prime objective behind acquiring a pan-sharpened image is to make it pragmatic for applications such as classification, recognition, and detection. Ideally, the distortion index called Spectral Angle Mapper (SAM) value should be close to zero so as to attain the optimum correlation between spectral bands of MS image. SAM is zero if the two spectral vectors corresponding to the images X and Y are parallel.

Under this assumption; to preserve the correlation between the MS image bands, a hypothesis is presented in the proposed method. The ratio of any two different spectral bands of HRMS image (X) should be equal to that of MS bands (Y),

$$\frac{X_i}{X_j} = \frac{\tilde{Y}_i}{\tilde{Y}_j}, 1 \leq i, j \leq B., i \neq j. \quad (12)$$

This constraint can be formulated as:

$$X_i \tilde{Y}_j - X_j \tilde{Y}_i = 0, j = 1, 2 \dots B., i \neq j. \quad (13)$$

An energy term, $J_3(X)$ is defined to preserve the desirable correlation information between multispectral bands. Further, $J_3(X)$ also reduces spectral distortion.

$$J_3(X) = \sum_{i=1}^B \sum_{j=1}^B \|X_i \tilde{Y}_j - X_j \tilde{Y}_i\|_2^2. \quad (14)$$

On combining three prior terms, $J_1(X)$, $J_2(X)$ and $J_3(X)$, the cost functional $J(X)$ for the proposed pan-sharpening algorithm is formulated as:

$$J(X) = \frac{1}{2} \sum_{i=1}^B \|Y_i - GX_i\|_2^2 + \alpha_1 \sum_{i=1}^B \|D(X_i - P) - r\|_1 + \alpha_0 \|\varepsilon(r)\|_1 + \frac{\lambda}{2} \sum_{i=1}^B \sum_{j=1}^B \|X_i \tilde{Y}_j - X_j \tilde{Y}_i\|_2^2 \quad (15)$$

where λ is a regularisation parameter, and its chosen value determines the relative contribution of inter-band correlation term.

3.4. Optimisation method

The proposed formulation given in Eq.(15) can be efficiently solved by the alternating direction method of multipliers (ADMM) (Gabay and Mercier 1975). ADMM solves the linearly constrained separable convex function of the form,

$$\min[\theta_1(x_1) + \theta_2(x_2)] \text{ subject to } A_1 x_1 + A_2 x_2 = b \quad (16)$$

$x_1 \in \phi_1$ and $x_2 \in \phi_2$.

$\theta_1 : \mathbb{R}^{n_1} \rightarrow \mathbb{R}$ and $\theta_2 : \mathbb{R}^{n_2} \rightarrow \mathbb{R}$ are closed proper convex functions; $\phi_1 \subset \mathbb{R}^{n_1}$ and $\phi_2 \subset \mathbb{R}^{n_2}$ are closed convex sets; $A_1 \in \mathbb{R}^{l \times n_1}$ and $A_2 \in \mathbb{R}^{l \times n_2}$ are given matrices and $b \in \mathbb{R}^l$ is a given vector. The Lagrangian is defined as $L(x_1, x_2; t) = \theta_1(x_1) + \theta_2(x_2) + \frac{\beta}{2} \|A_1 x_1 + A_2 x_2 - b - t\|_2^2$, t is the scaled Lagrange multiplier and β is a positive parameter. ADMM solves Eq. (16) in an iterative manner, and the process initialises with $x_2^0 = 0$ and $t^0 = 0$ as follows:

$$x_1^{k+1} = \operatorname{argmin}_{x_1} L(x_1, x_2^k; t^k)$$

$$x_2^{k+1} = \operatorname{argmin}_{x_2} L(x_1^{k+1}, x_2; t^k)$$

$$t^{k+1} = t^k + \beta(b - (A_1 x_1^{k+1} + A_2 x_2^{k+1}))$$

The pan-sharpening model described in Eq.(15) consists of a non-smooth l_1 term and can be amended by introducing auxiliary variables as

$$r = \begin{bmatrix} r_1 \\ r_2 \end{bmatrix} s = \begin{bmatrix} s_1 s_3 \\ s_3 s_2 \end{bmatrix}$$

The model presented in Eq.(15) is solved for each X_i value and can be presented as

$$\min_{X_i, P, v, s} \frac{1}{2} \|Y_i - GX_i\|_2^2 + \frac{1}{2} \sum_{i=1}^B \sum_{j=1}^B \|X_i \tilde{Y}_j - X_j \tilde{Y}_i\|_2^2 + \alpha_1 \|v\|_1 + \alpha_0 \|s\|_1 \quad (17)$$

subjected to $v_i = D(X_i - P) - r$, $s = \varepsilon(r)$.

The terms $\|v\|_1(\|s\|_1)$ are the sum of l_2 -norms (Frobenius norm) of all 2×1 vectors (2×2 matrices).

The application of ADMM (Guo *et al.* 2014b) results in the following parameters estimation:

$$v^{n+1} = \underset{v}{\operatorname{argmin}} \|v\|_1 + \frac{\mu_1}{2} \|v - (D(X - P)^n - r^n) - (v^n)\|_2^2 \quad (18)$$

$$s^{n+1} = \underset{s}{\operatorname{argmin}} \|s\|_1 + \frac{\mu_2}{2} \|s - \varepsilon(r^n) - (s^n)\|_2^2 \quad (19)$$

$$\begin{aligned} (X_i^{n+1}, p^{n+1}) = & \underset{X_i, P}{\operatorname{argmin}} \frac{1}{2} \|Y_i - GX_i\|_2^2 + \frac{1}{2} \sum_{i=1}^B \sum_{j=1}^B \|X_i \tilde{Y}_j - X_j \tilde{Y}_i\|_2^2 \\ & + \alpha_1 \frac{\mu_1}{2} \|v^{n+1} - (D(X_i - P) - r) - (v^n)\|_2^2 \\ & + \alpha_0 \frac{\mu_2}{2} \|s^{n+1} - \varepsilon(r^n) - (s^n)\|_2^2 \end{aligned} \quad (20)$$

$$v^{n+1} = v^n + \mu(D(X_i - P)^{n+1} - v^{n+1}) \quad (21)$$

$$s^{n+1} = s^n + \mu(\varepsilon(r^{n+1}) - s^{n+1}) \quad (22)$$

During each cycle of iterations from Eq.(18) to Eq.(22), Eq.(20) is a differentiable optimisation problem.

The v and s estimation subproblems specified in Eq.(21) and Eq.(22) can be solved using shrinkage operators as:

v -subproblem:

$$v^{n+1} = \operatorname{shrink}_1(D(X_i - P)^n - r^n + v^n, \frac{1}{\mu_1}) \quad (23)$$

where

$$\operatorname{shrink}_a(a, \frac{1}{\mu_1}) = \frac{a}{\|a\|_2} \cdot \max(\|a\|_2 - \frac{1}{\mu_1}, 0) \quad (24)$$

s -subproblem:

$$s^{n+1} = \operatorname{shrink}_b(\varepsilon(r^n) + s^n, \frac{1}{\mu_2}) \quad (25)$$

where

$$\operatorname{shrink}_b(b, \frac{1}{\mu_2}) = \frac{b}{\|b\|_F} \cdot \max(\|b\|_F - \frac{1}{\mu_2}, 0) \quad (26)$$

To obtain the solution of the differentiable part and the convergence analysis of ADMM algorithm with the comprehensive investigation, one can refer (Guo *et al.* 2014b).

4. Results and analysis

In this section, the proposed variational model for pan-sharpening is compared with some state-of-the-art methods at reduced-scale and full-scale: IHS (Tu *et al.* 2001) as the classical

CS-based method; AWLP (Otazu *et al.* 2005), MTF-GLP (Aiazzi *et al.* 2006) as the classical MRA-based methods; SR-LD (Li *et al.* 2013), SR-CD (Ayas *et al.* 2018) as the sparse representation-based methods; AVWP (Möller *et al.* 2012), DTV (Chen *et al.* 2014) and V-L1 (Chen *et al.* 2018) as the representative variational methods; PNN (Masi *et al.* 2016) and PNN plus (Scarpa *et al.* 2018) as deep learning-based methods.

To implement IHS, AWLP, and MTF-GLP methods, executable codes are available in the software package.¹ Three dictionaries are learned adaptively from the source images and the optimal size is considered as 1024 for each dictionary for the implementation of SR-LD method. The classical K-SVD algorithm is used to train the dictionaries with overlapped patches from the source PAN and MS images. The number of iterations during training is set as 25. The SR is implemented over the learned dictionary and the remaining parameters are taken as described in (Li *et al.* 2013). To achieve the pan-sharpened outcome with robust spatial and spectral features the dictionary size is selected as 2048 atoms in the SR-CD method implementation, and the number of iteration in the training phase is set as 25. The remaining parameters are considered as specified in (Ayas *et al.* 2018).

For the comparison purpose, the implementation of variational methods considers the optimal values for all the parameters to yield the best possible results. To validate the effectiveness of the proposed method, the visual and quantitative assessments are performed on IKONOS, Pléiades, and QuickBird sensor datasets. The resolution ratio between MS and PAN images is four for all the experimental datasets. All the methods are implemented in MATLAB R2013a, on a personal computer with intel CPU @3.10-GHz and 8-GB RAM.

The MATLAB package for PNN and PNN plus methods is available in Github.² The number of iterations in the PNN method is selected as 10. These two methods are implemented in MATLAB 2018a using deep learning toolbox.

4.1. Parameters selection

To implement the proposed algorithm in an efficient manner, several parameters need to be selected carefully. The regularisation parameters for TGV are selected to maintain an appropriate balance with the data synthesising fidelity term and inter-band correlation term. The image features are lost if more priority is given to the TGV term, whereas less priority results in residual noise in the fused image. The crucial regularisation parameter λ is tuned to give the best adaptation outcome between SAM and ERGAS. The value of λ influences the spectral quality of the fused image. The evolution characteristics of the parameter λ versus SAM and ERGAS for the datasets used in the reduced-scale evaluation are shown in Figure 1. Figure 2 presents the variation of Q4 and full-scale metrics D_1 and D_5 with respect to the variation in λ . Based on these observations, λ value is set as 0.9×10^{-3} for all the experiments. The quantitative results do not show any noticeable change for the variations in α_0 and α_1 . Hence, the other regularisation parameters are selected as $\alpha_0 = 10^{-2}$, $\alpha_1 = 10^{-3}$. The remaining parameters are set as $\mu_1 = 10^{-3}$, $\mu_2 = 10^{-5}$, since these parameters do not effect the spatial and spectral indices much. To maintain the balance between performance and complexity of the proposed algorithm, the number of iterations for the algorithm is selected as 25. Further, regulation of these parameters may produce better results; however, the currently selected parameters yield consistent results.

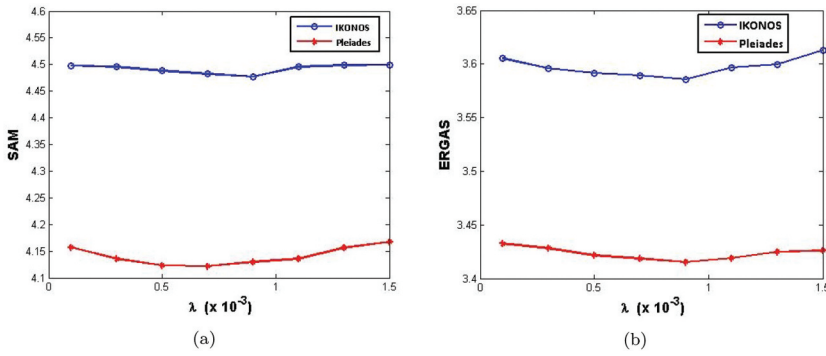


Figure 1. Evolution curves of SAM and ERGAS at reduced-scale against the variation in parameter λ (a) SAM Vs. λ (b) ERGAS Vs. λ .

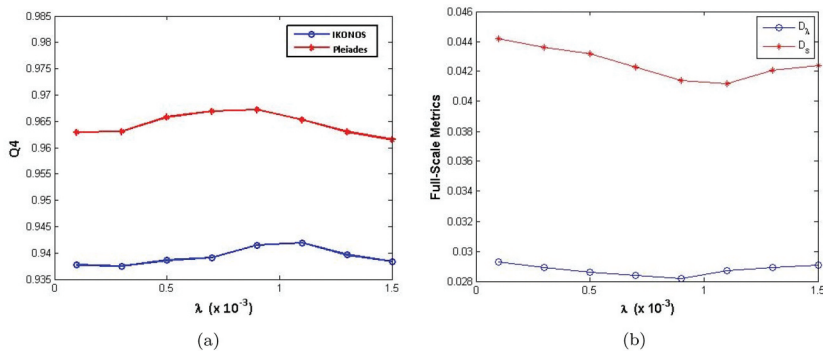


Figure 2. Evolution curves of Q4 (at reduced-scale), full-scale metrics against the variation in parameter λ (a) Q4 Vs. λ (b) D_I , D_S Vs. λ .

4.2. Reduced-resolution assessment

Since the reference high-resolution MS image is not available, Wald's protocol (Wald *et al.* 1997) is adapted to evaluate the quality of the fused image. The source images are down-sampled by a factor, which is equal to the resolution ratio between PAN and MS images and the original MS image is treated as a reference image. A considerable number of indices have been developed for spatial and spectral distortions of the pan-sharpened image. In this paper, root mean square error (RMSE), spectral angle mapper (SAM), Erreur Relative Globale Adimensionnelle de Synthèse (ERGAS), correlation coefficient (CC), and Universal Image Quality Index (UIQI) or Q-index (Q4) are used as quality metrics.

The PAN and MS images produced by IKONOS are of 1-m and 4-m resolutions, respectively. The size of images for experimentation is considered as 256×256 pixels. The visual outcomes of different methods for the IKONOS dataset at reduced-scale are presented in Figure 3. The corresponding quality metrics are reported in Table 1. Figure 3 (a and b) shows the PAN and MS images used for the experimental validation. Figure 3(c) presents the up-sampled MS image and termed as EXP. From the pan-sharpened images, it is observed that the IHS method yields an outcome with spectral distortion in the form

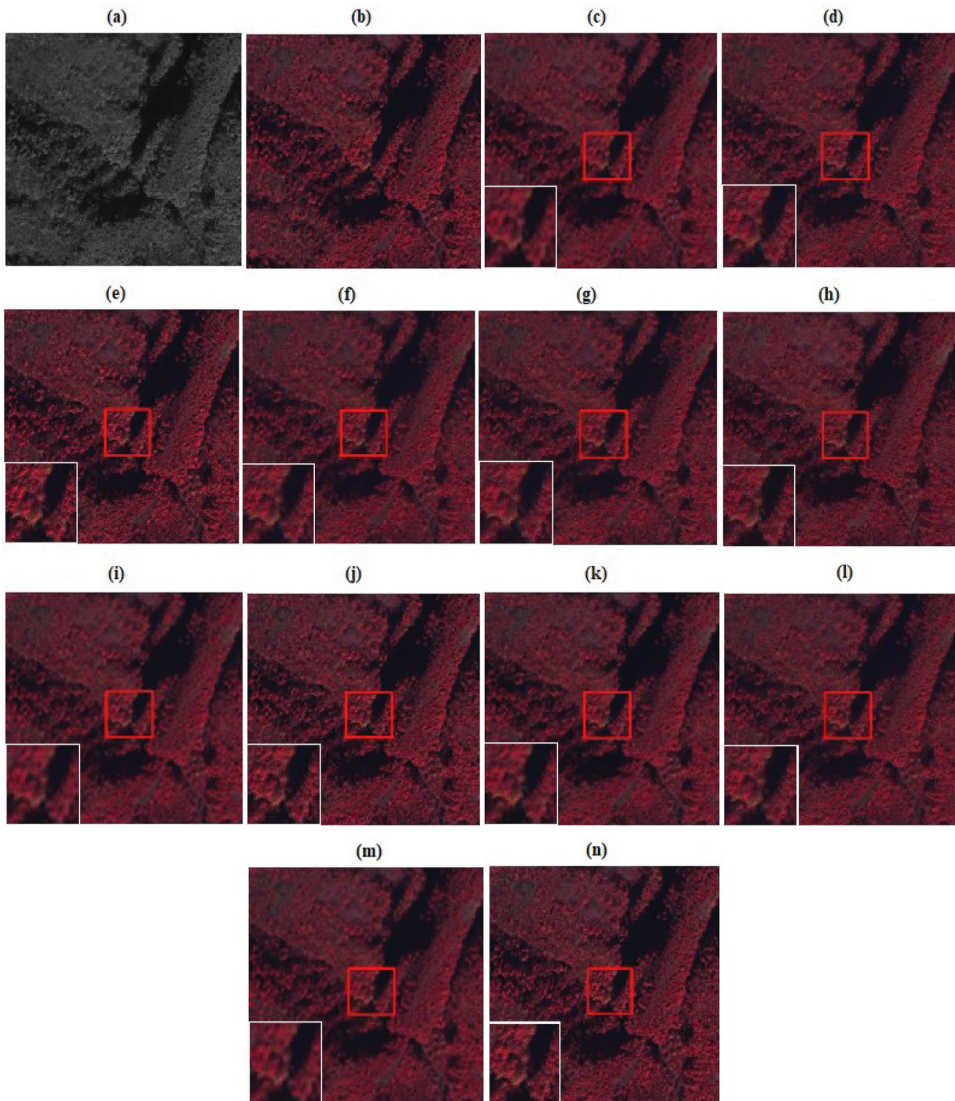


Figure 3. IKONOS dataset and experimental results by different methods (a) PAN image (b) Reference MS image (c) EXP (up-sampled MS image) (d) IHS (e) AWLP (f) MTF-GLP (g) AVWP (h) SR-LD (i) DTN (j) V-L1 (k) SR-CD (l) PNN (m) PNN plus (n) Proposed method.

of inconsistent colour and the AVWP method produces spatial and spectral distortions. The SR-CD, MTF-GLP, and AWLP methods exhibit fine spatial details. The evaluation of the outcomes of variational methods indicates a slight colour distortion. The outcomes of DTN and V-L1 methods are moderately good as these methods are able to preserve the sharp edges present in the original PAN image. The deep learning-based methods (PNN, PNN plus) show significant enhancement in visual results. The comprehensive perception manifests that the proposed method preserves fine spatial details than the other reported methods. For improved visualisation of spatial details, a part of the image is zoomed (encircled in a red box) and shown at the bottom left corner for every image. From [Table 1](#),

Table 1. Reduced-resolution quality metrics for IKONOS dataset.

Method	Q4	SAM	RMSE	ERGAS	CC
EXP	0.8251	5.6492	16.3371	5.1386	0.7917
IHS	0.8627	5.3537	15.6392	4.4137	0.8458
AWLP	0.9158	5.0845	15.1156	3.6324	0.9214
MTF-GLP	0.9231	5.1427	15.1093	3.5937	0.9276
AVWP	0.8885	5.2175	15.9173	4.5273	0.8721
SR-LD	0.8754	5.5146	16.1183	4.6259	0.8735
DTV	0.9237	4.6842	14.4131	<u>3.6521</u>	0.9283
V-L1	0.9314	4.7163	<u>14.3275</u>	<u>3.7128</u>	0.9351
SR-CD	0.9342	4.5739	<u>14.9748</u>	3.8862	0.9363
PNN	0.9318	4.6957	14.5306	3.7262	0.9354
PNN plus	<u>0.9367</u>	4.5781	14.3286	3.6643	0.9358
Proposed	0.9418	4.4753	14.1126	3.5861	0.9389

Note: The bold values represents optimal values for each quality metric

comparative analysis yield that the proposed method outperforms over all the reported methods for all the quality metrics considered. The second-best optimal value of performance measures is indicated with an underline.

The Pléiades³ dataset is collected by an aerial platform of an urban area of Toulouse (France). The resolution of the four MS bands is 60 cm and the corresponding high-resolution PAN image was simulated from the available green and red channels. The size of the images used for the implementation of pan-sharpening methods at the reduced-resolution is 300×300 pixels. Figure 4(b) shows the MS image covering an urban area, resampled to match the size of the PAN image. Figure 4(a) shows the corresponding PAN image. The visual outcomes of EXP, IHS, AWLP, MTF-GLP, AVWP, SR-LD, DTV, V-L1, SR-CD, PNN, PNN plus, and the proposed method are shown in Figure 4(c)-(n), respectively. The IHS method suffers from spectral distortion in the regions containing grass. It can be seen from Figure 4(g) that the AVWP method is unable to offer finer spatial resolution. The AWLP method and SR-based methods better preserve the colour in various regions of the fused image. It is observed from the results that AWLP, MTF-GLP, DTV, and SR-CD produce relatively enhanced visual quality. The visual outcomes of PNN and PNN plus methods exhibit noticeable improvement in preserving the requisite geometric features. The proposed method is superior in reducing the colour distortion and retaining the sharp spatial details than the other reported methods. Besides, the quantitative results for the Pléiades dataset are presented in Table 2. The proposed method achieves optimal values for all the metrics used in evaluation except for SAM. The obtained values of the performance measures validate the efficiency of the proposed method.

4.3. Full-resolution assessment

QuickBird produces the PAN and 4-band MS images at 0.7-m and 2.8-m spatial resolution, respectively. The QNR protocol (Alparone *et al.* 2008) is used for quantitative evaluations. Figure 5 presents another set of pan-sharpening results at full-resolution obtained from the QuickBird dataset. The quality metrics, namely, spectral distortion index (D_s), spatial distortion index (D_s) and QNR are reported in Table 3.

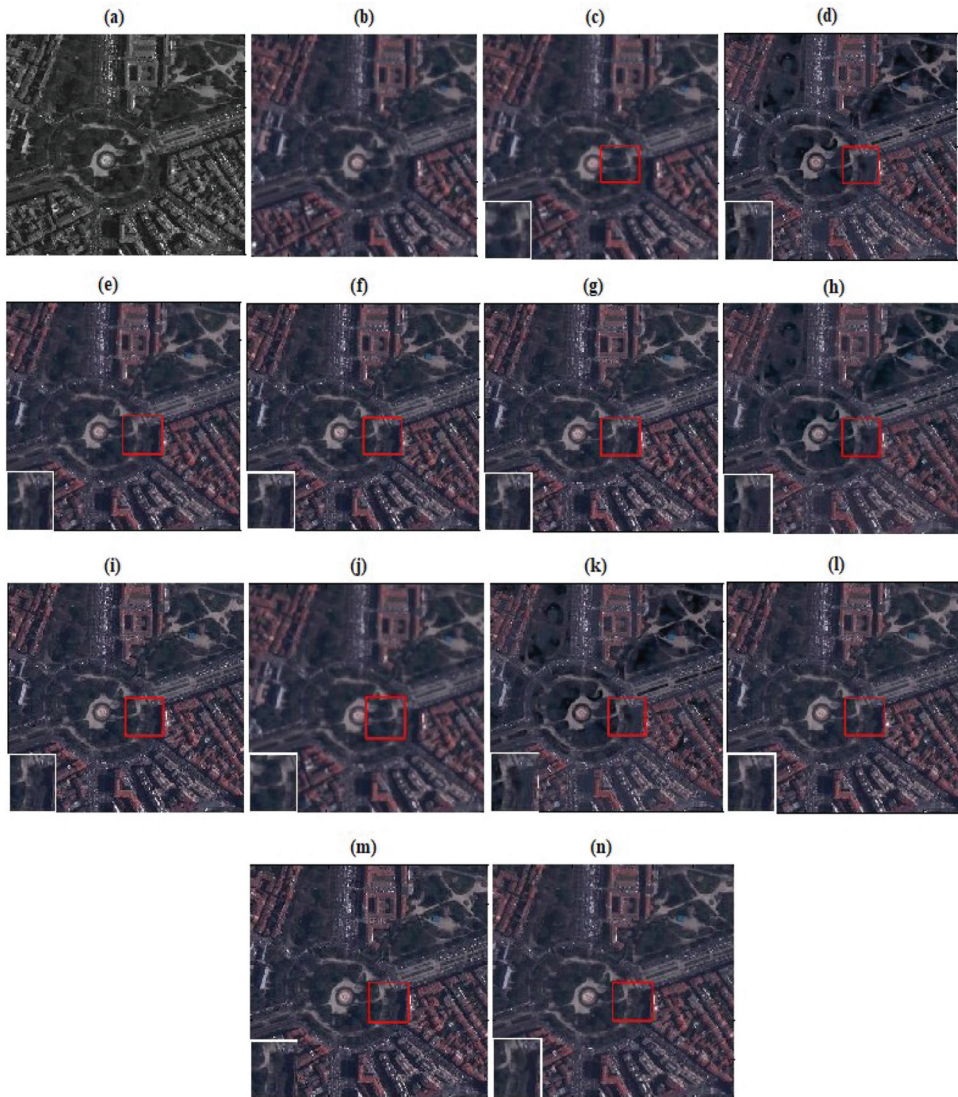


Figure 4. Pléiades dataset and experimental results by different methods (a) PAN image (300×300) (b) Reference MS image (c) EXP (up-sampled MS image) (d) IHS (e) AWLP (f) MTF-GLP (g) AVWP (h) SR-LD (i) DTV (j) V-L1 (k) SR-CD (l) PNN (m) PNN plus (n) Proposed method.

Figure 5(a and b) displays the full-resolution PAN and up-sampled MS images, respectively, of size 512×512 pixels. The outcomes of IHS, AVWP, and V-L1 exhibit slight colour change and blurring artefacts in the red coloured soil and highway portion of the image. The conventional AWLP and MTF-GLP outcomes preserve the spectral information. The outcome of the DTV method shows minute blocking artefacts. The pan-sharpened outcomes of SR-LD and SR-CD methods exhibit acceptable sharpness in preserving spatial details. The outcomes of PNN and PNN plus methods appear quite similar to the original MS image. The sharp features are retained by the fused outcomes of deep learning (PNN,

Table 2. Reduced-resolution quality metrics for Pléiades data set.

Method	Q4	SAM	RMSE	ERGAS	CC
EXP	0.7841	4.6853	13.7956	5.9562	0.8257
IHS	0.8495	4.9357	13.4531	5.1048	0.8573
AWLP	0.9413	4.4138	12.4176	3.5182	0.9587
MTF-GLP	0.9478	4.1735	12.3362	3.3174	0.9564
AVWP	0.9247	5.1123	12.4175	3.7293	0.9381
SR-LD	0.9483	4.3352	11.9731	3.4832	0.9653
DTV	0.9571	4.2673	10.9318	3.4536	0.9617
V-L1	0.9583	4.2759	10.6572	3.4369	0.9776
SR-CD	0.9654	4.0381	10.4729	3.4371	0.9743
PNN	0.9592	4.2463	10.5483	3.4376	0.9648
PNN plus	0.9648	4.0246	<u>10.3875</u>	<u>3.4296</u>	0.9765
Proposed	0.9673	<u>4.1736</u>	10.2358	3.4152	0.9782

Note: The significance of underline is the second optimal value for each quality metric.

PNN plus)-based methods. Moreover, the proposed method yields less spectral distortion and retains sharp edges over the other methods. The smaller value of D_l and D_s indicates less spectral distortion and spatial distortion, respectively. The higher value of QNR indicates enhanced global quality of the fused image. The proposed method offers the optimal values for D_l , D_s and QNR as reported in Table 3. Hence, the overall performance and efficacy of the proposed method are demonstrated by both the visual outcomes and quantitative results.

4.4. Reduced versus full-resolution quality assessment

Another dataset from QuickBird sensor is used to better demonstrate the efficiency of the proposed method at different resolutions. The original dataset considered is of size 1024×1024 pixels for PAN image and 256×256 pixels for MS image. The reduced and full-scale visual results for QuickBird dataset are presented in Figs.6 and 7, respectively.

For full-scale experimentation, QNR protocol is employed. The MS image is up-sampled to the resolution of PAN image, and the experimentation is performed on 1024×1024 sized source (PAN and MS) images.

One method from each category; IHS from CS, AWLP from MRA, SR-LD (with multiple dictionaries) and SR-CD (single compact dictionary) from SRbased, DTV from variational and PNN from deep learning-based methods are used for comparison. Three quality metrics, namely ERGAS, SAM, and Q4 at reduced resolution and QNR at full resolution are used for quantitative evaluation.

For fair visualisation of details both the image sets are displayed with the same size. The corresponding quality metrics are estimated and given in Table 4. For reduced-scale experiments, Wald's Protocol is used. The PAN and MS images are down-sampled by a ratio of four. Further, the MS image is up-sampled to the size of the PAN image and the original MS image is used as a reference image for comparison. The size of the source images for reduced-scale is 256×256 pixels.

The visual outcomes at reduced-scale are displayed in Figure 6. Figure 6(a and b) indicates the PAN and MS images used for experimentation, respectively. Figure 6(c) represents the reference MS image. Figure 6(d)-(i) presents the outcomes of different

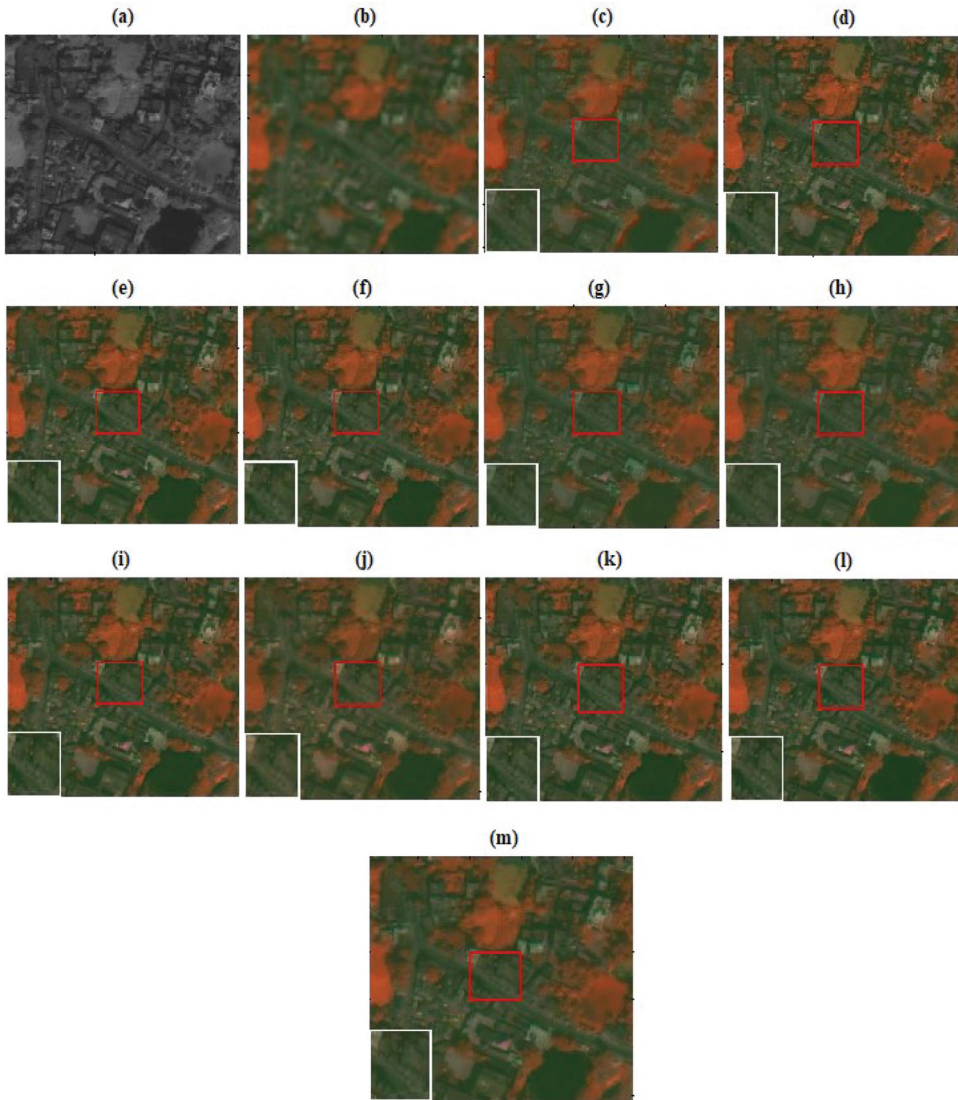


Figure 5. QuickBird dataset and experimental results by different methods (a) PAN image (512×512) (b) up-sampled MS image (c) IHS (d) AWLP (e) MTF-GLP (f) AVWP (g) SR-LD (h) DTV (i) V-L1 (j) SR-CD (k) PNN (l) PNN plus (m) Proposed method.

methods used for comparison. [Figure 6\(j\)](#) represents the outcome of the proposed method. The outcomes of SR-based methods, PNN and the proposed method are comparable in spatial and spectral qualities. The full-scale experiments presented in [Figure 7](#) follow the order of quality as results at reduced scale. The proposed method and PNN methods achieve better pan-sharpening quality than the CS- and MRA-based methods.

The quality metrics corresponding to the visual results shown in [Figures 6 and 7](#) are presented in [Table 4](#). The visual outcomes and the quality metrics obtained at different scales approve that the proposed method is insensitive to the scale and evaluation

Table 3. Full-resolution quality metrics for QuickBird data set.

Method	D_λ	D_s	QNR
EXP	0	0.1457	0.8544
IHS	0.0410	0.0576	0.9037
AWLP	0.0406	0.0480	0.9135
MTF-GLP	0.0372	0.0414	0.9229
AVWP	0.0428	0.0507	0.9087
SR-LD	0.0356	0.0513	0.9149
DTV	0.0338	0.0481	0.9197
V-L1	0.0315	0.0489	0.9211
SR-CD	0.0298	0.0453	0.9262
PNN	0.0301	0.0461	0.9252
PNN plus	0.0287	0.0416	0.9308
Proposed	0.0283	0.0409	0.9319

Note: The bold values represents optimal values for each quality metric

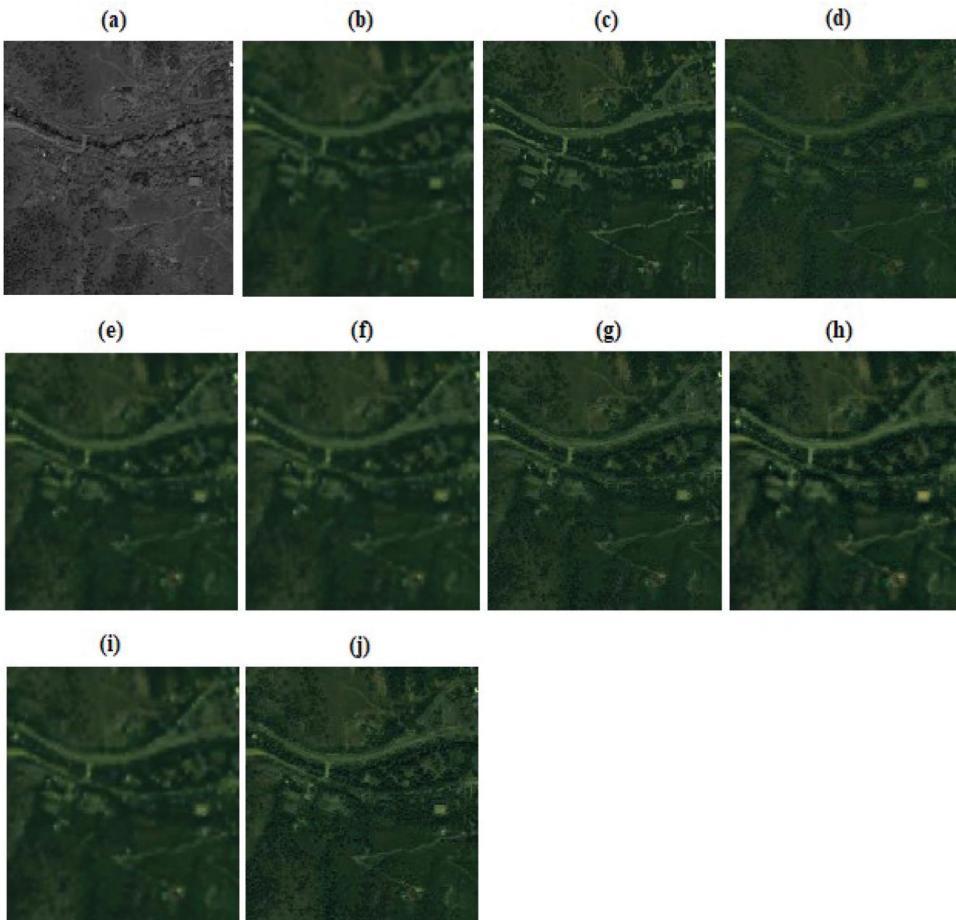


Figure 6. QuickBird dataset and experimental results by different methods at reduced-scale (a) PAN image (256×256) (b) up-sampled MS image (c) Reference MS image (d) IHS (e) AWLP (f) SR-LD (g) DTV (h) SR-CD (i) PNN (j) Proposed method.

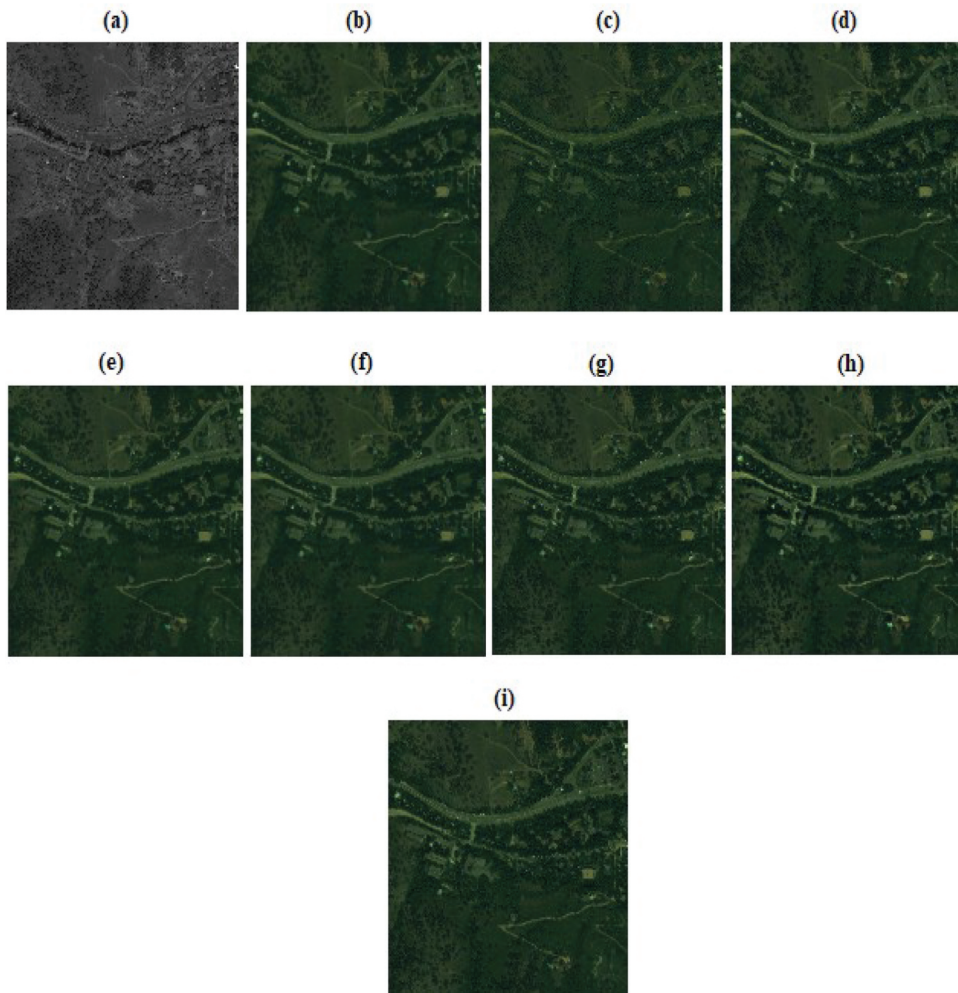


Figure 7. QuickBird dataset and experimental results by different methods at full-scale (a) PAN image (256×256) (b) up-sampled MS image (c) IHS (d) AWLP (e) SR-LD (f) DTV (g) SR-CD (h) PNN (i) Proposed method.

Table 4. Quality metrics for QuickBird dataset (reduced-scale and full-scale).

	Reduced-Scale				Full-Scale	
	ERGAS	SAM	Q4	D_λ	D_s	QNR
IHS	4.3262	4.5631	0.7835	0.0449	0.0535	0.9040
AWLP	4.2839	4.4124	0.8094	0.0425	0.0517	0.9079
SR-LD	4.1190	4.2371	0.8136	0.0397	0.0503	0.9119
DTV	3.9865	4.1791	0.8165	0.0372	0.0497	0.9149
SR-CD	3.7548	4.1017	0.8247	0.0358	0.0473	0.9186
PNN	3.7763	4.1126	0.8265	0.0342	0.0485	0.9190
Proposed	3.6240	4.1010	0.8352	0.0339	0.0479	0.9198

Note: The bold values represents optimal values for each quality metric

methodology. The quality metrics support the visual results and confirm that the

proposed method performs considerably better than other methods in spectral distortion reduction.

4.5. Comparison of algorithms execution time

The efficiency of all the considered methods is evaluated in terms of algorithm execution time measured in seconds. The average execution time is measured for the outcomes presented in Figures 3, 4, 5. The CS and MRA methods are recognised for relatively low execution time. It can be observed from Table 5 that IHS, AWLP, and MTF-GLP methods consume the least execution time among all the considered methods. Since the dictionary training process is computationally laborious, obviously the SR-based methods demand longer execution time. For the implementation of PNN and PNN plus methods (using MATLAB, CPU based), the number of iterations are considered as 10. The execution time is proportional to the amount of training data used and the number of iterations. The analysis based on these factors is out of scope for this paper. Hence, for fair comparison, the execution time for deep learning-based methods is not included in the list. The execution time for all the other considered methods is reported in Table 5. The proposed method is not as computationally efficient to the other reported variational methods like AVWP, DTV, and V-L1. However, the proposed method reduces the blocking artefacts and preserves spectral information at the cost of computational time.

From the perspective of accuracy and convergence speed, Figure 8 presents the relative error versus the iteration count for the proposed method. The relative error is evaluated as

$$\text{relativeerror} = \frac{\|X^k - Y\|}{\|Y\|} \quad (27)$$

where X^k is the pan-sharpened image obtained at k^{th} iteration and Y is the reference MS image. The relative error attains the least possible value for all the datasets after 25 iterations. The visual and quantitative results approve that the proposed method is superior to the methods, namely, AVWP, DTV, and V-L1 in terms of maintaining a trade-off between spatial and spectral qualities. From the execution time perspective, the proposed method is efficient than the reported SR-based methods.

5. Conclusion

In recent years, the variational scheme emerges as an attractive alternative for the pan-sharpening of multispectral images. This paper proposed a variational pan-

Table 5. Average execution time comparison of different methods (in seconds).

Method	Time(sec.)	Method	Time(sec.)
EXP	0	SR-LD	1486.0617
IHS	0.0119	DTV	39.7352
AWLP	0.1935	V-L1	116.2947
MTF-GLP	0.1385	SR-CD	652.3795
AVWP	95.3526	Proposed	218.6472

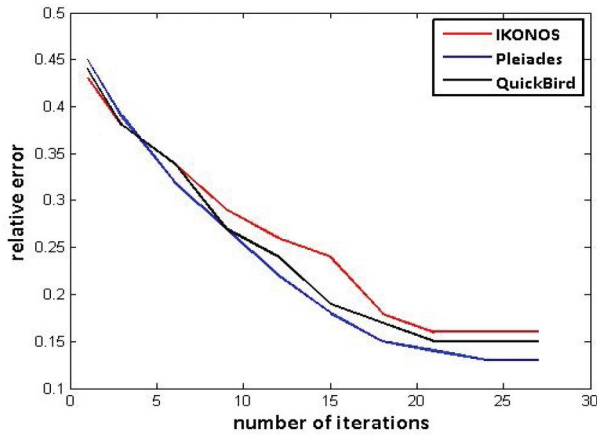


Figure 8. Convergence speed of the proposed method for the datasets utilised in experimentation.

sharpening model based on total generalised variation and inter-band correlation. The conventional total variation-based geometric terms result in a staircase effect in the pan-sharpened image. This work investigates a second-order TGV-based spatial difference term to reduce the geometric structural difference between HRMS image and PAN image. Further, the inter-band correlation term, inferred from spectral angle mapper (SAM) is used to reduce the spectral distortion. Moreover, an efficient optimisation algorithm called ADMM with an operator splitting framework is utilised to solve the proposed pan-sharpening model. For the comprehensive performance evaluation of the proposed scheme, the experiments are performed on reduced and full-resolution data. Furthermore, the proposed method is competitive with most of the SR, variational and deep learning-based methods and leads to satisfactory results compared to AVWP, DTV, V-L1, CNN, and CNN plus methods. The proposed work can be further extended to reduce the execution time and to exploit more reliable prior terms to efficiently characterise the relation between source and fused images.

Notes

1. <http://openremotesensing.net/kb/codes/pansharpening/>.
2. <https://github.com/sergiovitale/pansharpening-cnn-matlab-version>.
3. <http://openremotesensing.net/knowledgebase/a-critical-comparison-among-pansharpening-algorithms/>.

References

- Aiazzi, B., et al., 2006. MTF-tailored multiscale fusion of high-resolution MS and Pan imagery. *Photogrammetric Engineering & Remote Sensing*, 72 (5), 591–596. doi:10.14358/PERS.72.5.591
- Aiazzi, B., Baronti, S., and Selva, M., 2007. Improving component substitution pansharpening through multivariate regression of MS + Pan data. *IEEE Transactions on Geoscience and Remote Sensing*, 45 (10), 3230–3239. doi:10.1109/TGRS.2007.901007
- Alparone, L., et al., 2015. *Remote sensing image fusion*. Cleveland, Ohio: Crc Press.

- Alparone, L., et al., 2008. Multispectral and panchromatic data fusion assessment without reference. *Photogrammetric Engineering & Remote Sensing*, 74 (2), 193–200. doi:10.14358/PERS.74.2.193
- Amolins, K., Zhang, Y., and Dare, P., 2007. Wavelet based image fusion techniques — an introduction, review and comparison. *ISPRS Journal of Photogrammetry and Remote Sensing*, 62 (4), 249–263. doi:10.1016/j.isprsjprs.2007.05.009
- Ayas, S., Gormus, E.T., and Ekinci, M., 2018. An efficient pan sharpening via texture based dictionary learning and sparse representation. *IEEE Journal of Selected Topics in Applied Earth Observations and Remote Sensing* 11 (7), 2448–2460.
- Ballester, C., et al., 2006. A variational model for P+XS image fusion. *International Journal of Computer Vision*, 69 (1), 43–58. doi:10.1007/s11263-006-6852-x
- Bredies, K., Kunisch, K., and Pock, T., 2010. Total generalized variation. *SIAM Journal on Imaging Sciences*, 3 (3), 492–526. doi:10.1137/090769521
- Bredies, K. and Valkonen, T., 2011. Inverse problems with second-order total generalized variation constraints. In: 9th International Conference on Sampling Theory and Applications, Singapore, 2011.
- Chavez, P., et al. 1991. Comparison of three different methods to merge multiresolution and multispectral data- Landsat TM and SPOT panchromatic. *Photogrammetric Engineering and Remote Sensing*, 57, 295–303.
- Chen, B., Huang, B., and Xu, B., 2017. Multi-source remotely sensed data fusion for improving land cover classification. *ISPRS Journal of Photogrammetry and Remote Sensing*, 124, 27–39. doi:10.1016/j.isprsjprs.2016.12.008
- Chen, C., et al., 2014. Image fusion with local spectral consistency and dynamic gradient sparsity. In: Proceedings of the IEEE Conference on Computer Vision and Pattern Recognition, Greater Columbus Convention Center in Columbus, Ohio, June 24–27, 2014, pp. 2760–2765.
- Chen, C., et al., 2018. A novel variational model for pan-sharpening based on l1 regularization. *Remote Sensing Letters*, 9 (2), 170–179. doi:10.1080/2150704X.2017.1410292
- Cheng, J., et al., 2015. Remote sensing image fusion via wavelet transform and sparse representation. *ISPRS Journal of Photogrammetry and Remote Sensing*, 104, 158–173. doi:10.1016/j.isprsjprs.2015.02.015
- Cheng, M., Wang, C., and Li, J., 2014. Sparse representation based pansharpening using trained dictionary. *IEEE Geoscience and Remote Sensing Letters*, 11 (1), 293–297. doi:10.1109/LGRS.2013.2256875
- Duran, J., et al., 2014. A nonlocal variational model for pansharpening image fusion. *SIAM Journal on Imaging Sciences*, 7 (2), 761–796. doi:10.1137/130928625
- Duran, J., et al., 2017. A survey of pansharpening methods with a new band-decoupled variational model. *ISPRS Journal of Photogrammetry and Remote Sensing*, 125, 78–105. doi:10.1016/j.isprsjprs.2016.12.013
- Gabay, D. and Mercier, B., 1975. *A dual algorithm for the solution of non linear variational problems via finite element approximation*. Institut de recherche d’informatique et d’automatique. Great Britain: Pergamon Press.
- Ghassemian, H., 2016. A review of remote sensing image fusion methods. *Information Fusion*, 32, 75–89. doi:10.1016/j.inffus.2016.03.003
- Gogineni, R. and Chaturvedi, A., 2018. Sparsity inspired pan-sharpening technique using multi-scale learned dictionary. *ISPRS Journal of Photogrammetry and Remote Sensing*, 146, 360–372. doi:10.1016/j.isprsjprs.2018.10.009
- Guo, W., Qin, J., and Yin, W., 2014a. A new detail-preserving regularization scheme. *SIAM Journal on Imaging Sciences* 7, 1309–1334.
- Guo, W., Qin, J., and Yin, W., 2014b. A new detail-preserving regularization scheme. *SIAM Journal on Imaging Sciences*, 7 (2), 1309–1334. doi:10.1137/120904263
- He, X., et al., 2014. A new pansharpening method based on spatial and spectral sparsity priors. *IEEE Transactions on Image Processing*, 23 (9), 4160–4174. doi:10.1109/TIP.2014.2333661
- Huang, W., et al., 2015. A new pan-sharpening method with deep neural networks. *IEEE Geoscience and Remote Sensing Letters*, 12 (5), 1037–1041. doi:10.1109/LGRS.2014.2376034

- Hussain, M., et al., 2013. Change detection from remotely sensed images: from pixel-based to object-based approaches. *ISPRS Journal of Photogrammetry and Remote Sensing*, 80, 91–106. doi:10.1016/j.isprsjprs.2013.03.006
- Imani, M. and Ghassemian, H., 2017. Pansharpening optimisation using multiresolution analysis and sparse representation. *International Journal of Image and Data Fusion*, 8, 270–292.
- Jiang, C., et al., 2012. A practical compressed sensing-based pan-sharpening method. *IEEE Geoscience and Remote Sensing Letters*, 9 (4), 629–633. doi:10.1109/LGRS.2011.2177063
- Jiang, C., et al., 2014. Two-step sparse coding for the pan-sharpening of remote sensing images. *IEEE Journal of Selected Topics in Applied Earth Observations and Remote Sensing*, 7 (5), 1792–1805. doi:10.1109/JSTARS.2013.2283236
- Knoll, F., et al., 2011. Second order total generalized variation (TGV) for MRI. *Magnetic Resonance in Medicine*, 72 (2), 480–491. doi:10.1002/mrm.22595
- Laben, C.A. and Brower, B.V., 2000. *Process for enhancing the spatial resolution of multispectral imagery using pan-sharpening*. US Patent 6,011,875.
- Li, M., et al., 2016. Urban land use extraction from very high resolution remote sensing imagery using a bayesian network. *ISPRS Journal of Photogrammetry and Remote Sensing*, 122, 192–205. doi:10.1016/j.isprsjprs.2016.10.007
- Li, S. and Yang, B., 2011. A new pan-sharpening method using a compressed sensing technique. *IEEE Transactions on Geoscience and Remote Sensing*, 49 (2), 738–746. doi:10.1109/TGRS.2010.2067219
- Li, S., Yin, H., and Fang, L., 2013. Remote sensing image fusion via sparse representations over learned dictionaries. *IEEE Transactions on Geoscience and Remote Sensing*, 51 (9), 4779–4789. doi:10.1109/TGRS.2012.2230332
- Ling, Y., et al., 2007. FFT-enhanced IHS transform method for fusing high-resolution satellite images. *ISPRS Journal of Photogrammetry and Remote Sensing*, 61 (6), 381–392. doi:10.1016/j.isprsjprs.2006.11.002
- Lotfi, M. and Ghassemian, H., 2018. A new variational model in texture space for pansharpening. *IEEE Geoscience and Remote Sensing Letters*, 15 (8), 1269–1273. doi:10.1109/LGRS.2018.2836951
- Ma, L., et al., 2019. Deep learning in remote sensing applications: A meta-analysis and review. *ISPRS Journal of Photogrammetry and Remote Sensing*, 152, 166–177. doi:10.1016/j.isprsjprs.2019.04.015
- Masi, G., et al., 2016. Pansharpening by convolutional neural networks. *Remote Sensing*, 8 (7), 594. doi:10.3390/rs8070594
- Möller, M., et al., 2012. A variational approach for sharpening high dimensional images. *SIAM Journal on Imaging Sciences*, 5 (1), 150–178. doi:10.1137/100810356
- Otazu, X., et al., 2005. Introduction of sensor spectral response into image fusion methods. application to wavelet-based methods. *IEEE Transactions on Geoscience and Remote Sensing*, 43, 2376–2385.
- Palsson, F., Sveinsson, J.R., and Ulfarsson, M.O., 2014. A new pansharpening algorithm based on total variation. *IEEE Geoscience and Remote Sensing Letters*, 11 (1), 318–322. doi:10.1109/LGRS.2013.2257669
- Rahmani, S., et al., 2010. An adaptive IHS pan-sharpening method. *IEEE Geoscience and Remote Sensing Letters*, 7 (4), 746–750. doi:10.1109/LGRS.2010.2046715
- Ranchin, T., et al., 2003. Image fusion—the ARSIS concept and some successful implementation schemes. *ISPRS Journal of Photogrammetry and Remote Sensing*, 58, 4–18.
- Saeedi, J. and Faez, K., 2011. A new pan-sharpening method using multiobjective particle swarm optimization and the shiftable contourlet transform. *ISPRS Journal of Photogrammetry and Remote Sensing*, 9 (3), 365–381. doi:10.1016/j.isprsjprs.2011.01.006
- Scarpa, G., Vitale, S., and Cozzolino, D., 2018. Target-adaptive CNN-based pansharpening. *IEEE Transactions on Geoscience and Remote Sensing*, 56 (9), 5443–5457. doi:10.1109/TGRS.2018.2817393
- Tu, T.M., et al., 2001. A new look at IHS-like image fusion methods. *Information Fusion*, 2 (3), 177–186. doi:10.1016/S1566-2535(01)00036-7
- Vicinanza, M.R., et al., 2015. A pansharpening method based on the sparse representation of injected details. *IEEE Geoscience and Remote Sensing Letters*, 12, 180–184.

- Vivone, G., *et al.*, 2015. A critical comparison among pansharpening algorithms. *IEEE Transactions on Geoscience and Remote Sensing*, 53 (5), 2565–2586. doi:[10.1109/TGRS.2014.2361734](https://doi.org/10.1109/TGRS.2014.2361734)
- Wald, L., Ranchin, T., and Mangolini, M., 1997. Fusion of satellite images of different spatial resolutions: assessing the quality of resulting images. *Photogrammetric Engineering and Remote Sensing*, 63, 691–699.
- Xu, Q., Zhang, Y., and Li, B., 2014. Recent advances in pansharpening and key problems in applications. *International Journal of Image and Data Fusion*, 5 (3), 175–195. doi:[10.1080/19479832.2014.889227](https://doi.org/10.1080/19479832.2014.889227)
- Zhou, X., *et al.*, 2014. A GHS-based spectral preservation fusion method for remote sensing images using edge restored spectral modulation. *ISPRS Journal of Photogrammetry and Remote Sensing*, 88, 16–27. doi:[10.1016/j.isprsjprs.2013.11.011](https://doi.org/10.1016/j.isprsjprs.2013.11.011)
- Zhu, X.X. and Bamler, R., 2013. A sparse image fusion algorithm with application to pan-sharpening. *IEEE Transactions on Geoscience and Remote Sensing*, 51 (5), 2827–2836. doi:[10.1109/TGRS.2012.2213604](https://doi.org/10.1109/TGRS.2012.2213604)